Thermal transport in nanocrystalline materials

Zhanrong Zhong and Xinwei Wang[a)]
Department of Mechanical Engineering, N104 Walter Scott Engineering Center, The University of Nebraska-Lincoln, Lincoln, Nebraska 68588-0656

(Received 20 November 2005; accepted 10 July 2006; published online 23 August 2006)

In this work, thermal transport in nanocrystalline materials is studied using large-scale equilibrium molecular dynamics simulation. Nanocrystalline materials with different grain sizes are studied to explore how and to what extent the size of nanograins affects the thermal conductivity and specific heat. Substantial thermal conductivity reduction is observed and the reduction is stronger for nanocrystalline materials with smaller grains. On the other hand, the specific heat of nanocrystalline materials shows little change with the grain size. Based on the calculated thermal conductivity, the thermal resistance at grain boundaries is calculated and found to be in the order of 10^{-9} m^2 K/W. The simulation results are compared with the thermal transport in freestanding nanograins based on molecular dynamics simulation. Further discussions are provided to explain the fundamental physics behind the observed thermal phenomena in this work. © *2006 American Institute of Physics*.
[DOI: 10.1063/1.2266206]

I. INTRODUCTION

Nanocrystalline materials are the materials that consist of individual grains of the order of several to hundreds of nanometers. Due to the small size of the grains, the thermal transport in nanocrystalline materials can be reduced significantly by the strong grain boundary scattering of energy carriers, which makes the thermal conductivity of the bulk counterpart not valid in heat transfer study.

To date, a large number of experimental investigations have been conducted to study the thermal transport in nanocrystalline materials. Using an effective medium approach, Nan and Birringer[1] experimentally determined the grain boundary resistance in coarse-grained polycrystalline SiGe and BiTe/SbTe alloys. In recent works by Eastman and co-workers,[2,3] effects of energy carrier (phonon) scattering on thermal transport within nanograins and on thermal transport across the nanograin interface have been investigated. By studying the variation of the effective thermal conductivity of nanocrystalline zirconia with the size of nanograins and temperature, they reported a reduced thermal conductivity of the nanograin itself due to phonon scattering at the grain interface. Furthermore, their experimental results and fitting data led to an interfacial resistance in the order of 10^{-9}–10^{-8} m^2 K/W. The density, Young's modulus, and the thermal diffusivity of nanocrystalline diamond films were also experimentally investigated.[4]

In addition to the experimental work, various numerical investigations in this area have also been reported in recent years. Using molecular dynamics (MD) simulation, it was found that the grain boundary structure of nanocrystalline copper (nc-Cu) was similar to that of large grain polycrystals.[5,6] Although grain sizes within nc-Cu are not strongly related to crystallographic orientations,[7] abrupt change of crystallographic orientations existed across grain boundaries, while no evident change was found for lattice spacing.[8] The structure of nc-Cu, which features a large volume fraction of atoms within grain boundaries, results in unique properties that include much increased microhardness (up to six times),[9,10] extreme extensibility (elongation exceeding 5000%) without strain hardening,[11–13] and much reduced thermoelectric power.[14] Thermal transport in nc-Cu is strongly related to the electrical transport because conduction electrons sustain both processes. It was found that nanograins within nc-Cu substantially reduced the mean free path of electrons and increased the electrical resistivity.[14,15]

In this work, MD simulation is conducted to study the thermal transport in nanocrystalline argon. Due to the large number of atoms under consideration, parallel computation is employed. A numerical technique is developed to construct the nanocrystalline material in a fast and efficient way. Nanocrystalline materials with different grain sizes are studied to explore how and to what extent the size of nanograins affects their thermophysical properties. The simulation results are compared with those for freestanding nanograins calculated in our previous work. Further discussions and physical interpretation of the observed thermal phenomena are also provided.

II. METHODOLOGY

A. Basis of MD simulation

The basis of MD simulation is to simulate the trajectory of each atom in a system by solving the Newtonian equation combined with the expression of potential energy. The positions, forces, and velocities of the atoms under study can be obtained at each time step. For each atom, the Newtonian equation governs its movement as follows:

$$m_i \frac{d^2 r_i}{dt^2} = \sum_{i \neq j}^{N} F_{ij}, \tag{1}$$

where m_i is the mass of atom i, r_i is its position, and N is the total number of atoms in the system. F_{ij} is the interaction

[a)]Author to whom correspondence should be addressed; FAX: (402) 472-1465; electronic mail: xwang3@unl.edu

TABLE I. Values of the parameters used in this work.

Parameters	Value
LJ well depth parameter, ε	1.653×10^{-21} J
LJ equilibrium separation, σ	0.3406 nm
Argon atomic mass, m	6.63×10^{-26} kg
Boltzmann's constant, k_B	1.38×10^{-23} J/K
Lattice constant, a	0.5355 nm
Cutoff distance, r_{cut}	0.8515 nm
Temperature, T	30 K
Size of the nanograin	2.142–10.71 nm
Size of the total domain	8.568–42.84 nm
Time step, Δt	5 fs

force between atoms i and j, which is derived from the Lennard-Jones (LJ) 12-6 potential function[16] for the material (argon) studied in this work:

$$\phi_{ij}(r_{ij}) = 4\varepsilon\left[\left(\frac{\sigma}{r_{ij}}\right)^{12} - \left(\frac{\sigma}{r_{ij}}\right)^{6}\right], \tag{2}$$

$$F_{ij} = -\frac{\partial\phi_{ij}}{\partial r_{ij}}, \tag{3}$$

where r_{ij} is the distance between atoms i and j ($r_{ij}=r_i-r_j$), ϕ_{ij} is the LJ potential between these two atoms, ε is the LJ well depth, and σ is the equilibrium separation parameter. When r_{ij} is much larger than σ, the two terms in the potential expression will be negligible. In order to improve the computation efficiency, a widely used cutoff distance $r_{ij}=2.5\sigma$ (Ref. 17) is employed. If the distance between two atoms is larger than the cutoff distance, the force and potential between them will be taken as zero.

Several methods have been developed to solve Eqs. (1)–(3). In this work, the widely used Verlet algorithm is employed, in which the half-step leap-frog scheme is used. The time step should be chosen to be much smaller than the phonon relaxation time. In our calculation, the time step takes 5 fs, which is much smaller than the typical value of the relaxation time of phonons ($\sim$1 ps) in argon crystal. Values of the parameters used in this work are summarized in Table I.

In this work, the static Green-Kubo method is used to calculate the thermal conductivity[18]

$$k_m = \frac{V}{k_B T^2}\int_0^\infty \langle q_m(0)q_m(t)\rangle dt, \tag{4}$$

where V is the volume of the system, k_B is Boltzmann's constant, and q_m is the heat flux in the m ($m=x$, y, or z) direction. From the equation of energy conservation

$$\frac{1}{V}\frac{\partial E}{\partial t} + \nabla\cdot\mathbf{q} = 0 \tag{5}$$

and the expression of the energy of an atom in terms of the atomic kinetic and potential energies

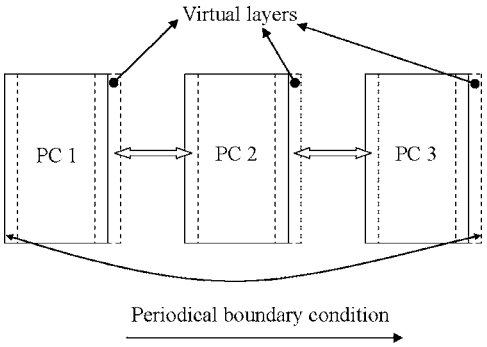

FIG. 1. Principle of parallel computation.

$$E_i = \sum_{j=1}^{N}\frac{1}{2}\phi_{ij} + \frac{1}{2}m\nu_i^2, \tag{6}$$

the expression of heat flux q_m is derived as

$$q_m V = \sum_{i=1}^{N}\nu_{im}E_i + \frac{1}{2}\sum_{i=1}^{N}\sum_{j>i}^{N} r_{ijm}\cdot F_{ijm}(\nu_{im}+\nu_{jm}). \tag{7}$$

In order to calculate the specific heat, the fluctuation in the total energy needs to be computed, which includes both the kinetic and potential components[16]

$$\langle\delta E^2\rangle = \frac{3}{2}N(k_B T)^2 + \langle\delta u^2\rangle, \tag{8}$$

where u is the potential energy. The second term in Eq. (8) is the fluctuation in the potential energy and has the expression of

$$\langle\delta u^2\rangle = \langle u^2\rangle - \langle u\rangle^2. \tag{9}$$

The specific heat is determined by the fluctuation in the total energy as[16]

$$k_B T^2 C_\nu = \langle\delta E^2\rangle \tag{10}$$

In this work, a large number of atoms are needed in order to simulate the nanocrystalline material with a number of nanograins inside. The largest sample has about 2 000 000 atoms. Over 400 000 time steps are used in each case. In order to make the computation feasible, parallel algorithm is used. The principle of parallel computation is briefly demonstrated in Fig. 1. The entire computational domain is divided into small subdomains, each of which is processed by one computing node. Each subdomain is divided into several layers. The width/thickness of each layer is equal to, or a little larger than, the cutoff distance, which means that only the atoms in the edge layer will interact with the atoms in the subdomain next to it. At each time step, only the position information about the atoms in the left layer of each subdomain need to be transferred to the left computer and become a virtual layer for the left computing node. After force calculation, the calculated force will be returned to the right computing node. The parallel computation is conducted on the parallel computer "Prairie Wind" in the Micro/Nanoscale Thermal Science Laboratory at UNL. This computer consists of 52 high-performance computing nodes.

B. Numerical construction of nanocrystalline materials

The first step of this work is to create the structure of the nanocrystalline material. Some methods have been reported in the past for constructing nanocrystalline materials. In the work by Peng *et al.*,[5] an initial system consisting of seven spherical clusters was first constructed. Each cluster had a randomly chosen crystallographic orientation. Then the system was relaxed for hundreds of picoseconds to obtain nanocrystalline structure. The disadvantage of this method is that much free space exists among nanograins, leading to a low material density. Swygenhoven *et al.*[6] created nanocrystalline samples based on unconstrained and constrained stochastic methods. In their work, the domain was filled with nanograins grown from a seed with random locations and crystallographic orientations until the grains overlap. Another method was reported by Phillpot *et al.*[19] In their method, a liquid system was quenched and the liquid crystallized around arranged seeds in space. In order to have nanograins, each seed was chosen to have different crystallographic orientations. It took quite a long time for the whole system to crystallize to form a nanocrystalline material.

The numerical technique developed in this work is similar to that by Swygenhoven *et al.*,[6] but with a much more controlled grain size uniformity in order to explore the grain size effect on thermophysical properties. In this work, free boundary conditions are used in all the directions. Several seeds are first placed inside the physical domain of interest for numerical crystal growth. In order to investigate the effect of the nanograin size on thermal transport, the seeds are distributed uniformly in space to keep the size of each nanograin close to each other. The orientation of the seeds is rotated around the z direction by randomly chosen angles. As a result, each seed will grow with different crystallographic orientations. In numerical growth, the growing speed of the grain is controlled to be uniform in every direction and all the grains have the same speed of growth. If the distance between any two atoms (each of which belongs to a different grain) becomes less than 90% of the nearest interatomic distance in argon crystal, the grain will stop growing in this direction. Each grain keeps growing until the entire domain of interest is full of atoms. The grain growth is controlled to construct a sample of cubic shape. Figure 2 shows one of the x-y plane configurations for a nanocrystalline argon just after growth. The layer thickness shown in Fig. 2 in the z direction is the nearest distance among atoms (0.38 nm). This layer is located around the middle of the sample in the z direction. There are four nanograins in each direction and the size of each nanograin is ~6.246 nm. It is evident that each nanograin has different orientation, and small gaps exist among nanograins.

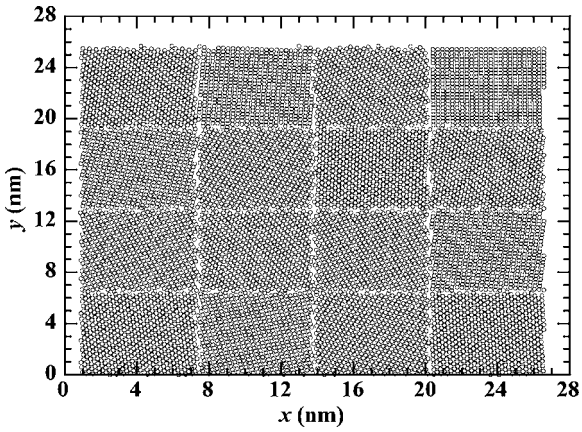

FIG. 2. Initial structure of an x-y plane in nanocrystalline argon consisting of 64 nanograins of 6.426 nm size. The thickness (z direction) of this plane is 0.38 nm.

III. RESULTS AND DISCUSSION

A. Structure of nanocrystalline materials

The material under study is argon nanocrystal, which has the fcc structure, and the temperature is set to 30 K to keep it in solid state. As described in Sec. II B, a numerical method was developed to create the nanocrystalline structure. After the initial construction, a process of equilibrium calculation lasting 400 ps is performed to make the system reach the thermal equilibrium state. For the case shown in Fig. 2, the configuration after equilibrium calculation is illustrated in Fig. 3, where the thickness in the z direction is 0.38 nm. Due to a large number of small sliding events at grain boundaries, the boundaries become much different from the initial ones shown in Fig. 2. One direct consequence of the sliding events at grain boundaries is the increase in the density of the nanocrystalline material. Figure 4 shows the density of the nanocrystalline argon with the initial configuration and after equilibrium calculation. For purpose of comparison, the density of single crystal argon is also displayed in Fig. 4. Figure 4 indicates that after thermal equilibrium calculation, the nanocrystalline material becomes denser. The density of the nanocrystalline material is strongly affected by the grain size. The result shown in Fig. 4 demonstrates that the density of the nanocrystalline material decreases when the grain size becomes smaller. This is largely due to the significant grain boundary to volume ratio for nanocrystalline materials with small grains inside. For the material at the grain boundary, the local disorder makes the local density smaller than that of the bulk counterpart. Therefore, larger grain boundary to volume ratio will result in lower density of the entire material.

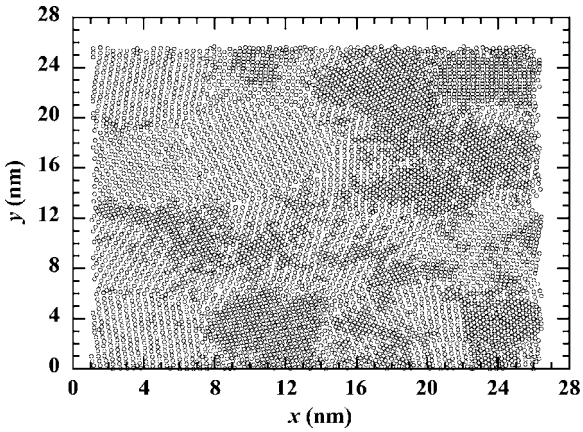

FIG. 3. The configuration of atoms in an x-y plane after equilibrium calculation. The thickness (z direction) of this plane is 0.38 nm.

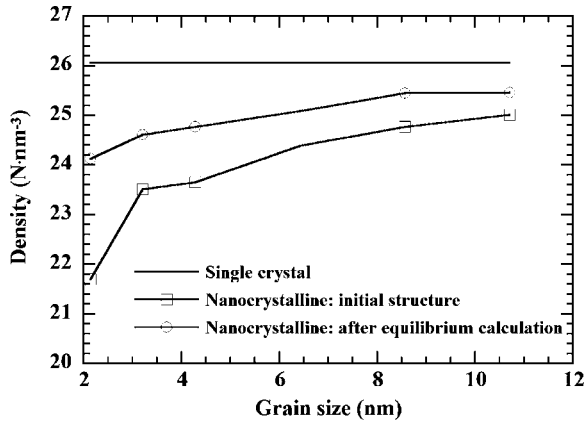

FIG. 4. Variation of density against the grain size for the nanocrystalline material in comparison with the single crystal counterpart.

For the nanocrystalline material with the smallest grain size (~2 nm) studied in this work, its density is about 92% of the bulk one. This small density reduction ensures that the thermal conductivity reduction observed in this work (discussed in Sec. III C) is not only attributed to density reduction, but also to phonon scattering at grain boundaries.

As expected, the unique structure of nanocrystalline materials could lead to significant thermophysical property changes in comparison with the bulk counterpart. Before exploring the thermophysical properties of nanocrystalline materials, it would be of interest to investigate their structure to understand the physics behind the physical property change. In this section, the structure of the nanocrystalline materials of interest is studied by examining their radial distribution function. The radial distribution function $g(r)$ is the probability of occurrence of an atom at a distance r from another atom. So the calculation of $g(r)$ involves averaging the number of particles at a distance r from any particle in the system and dividing that number by the volume $4\pi r^2 dr$. In this work, the maximum distance r_{max} under study is 6σ and dr is chosen as $r_{max}/100$. The radial distribution function of nanocrystalline argon with three different grain sizes is shown in Fig. 5. The radial distribution function is calculated after the nanocrystalline material reaches the thermal equilibrium state. For comparison, the radial distribution function of a single argon crystal film at the same temperature is displayed in each figure as well. The length of the argon film in the x and y directions is 10.71 nm, with periodical boundary conditions. The thickness of the film is 17.14 nm, with free boundary conditions in the thickness direction. The radial distribution function is calculated after the equilibrium calculation (400 ps) of the film. Taking the nanocrystalline argon consisting of 2.14 nm grains as an example, it is observed that the values of the peaks in nanocrystalline materials are smaller than those of single crystal argon. Since these peaks reflect the crystalline structure of the material, this observation reflects the structural disorder at the grain boundaries among nanograins. Besides the value of the peaks, it is also observed that the width (span) of the peaks is wider in nanocrystalline materials than in single crystal argon. This is induced by the structural disorder at the grain boundaries. With increasing grain size, the radial distribution

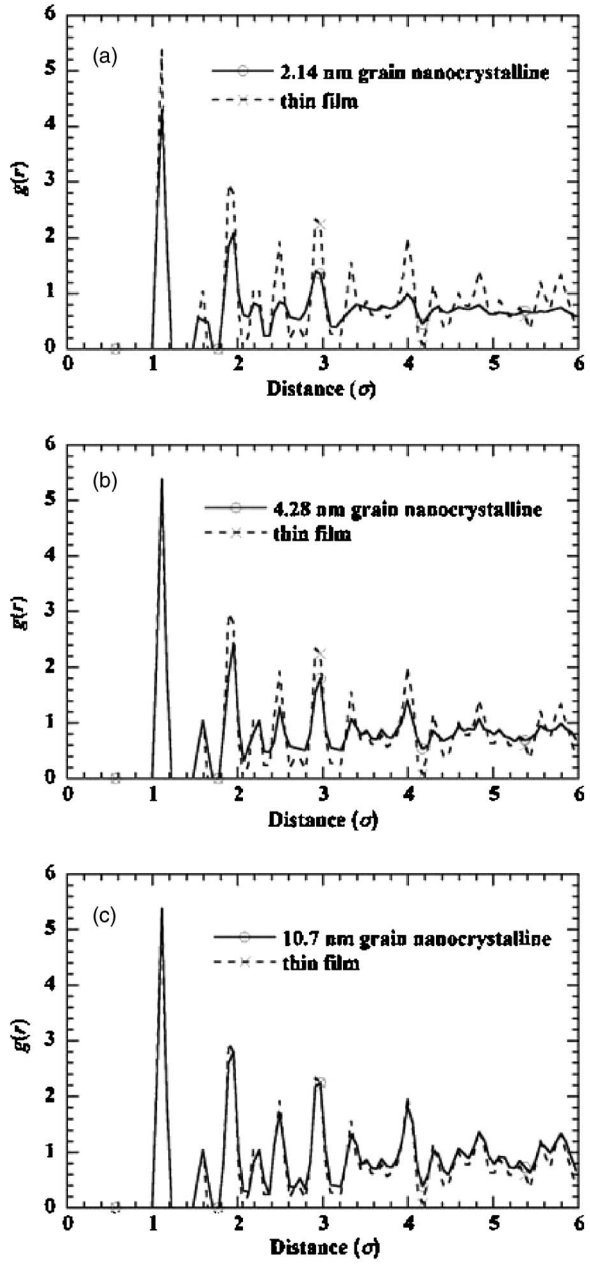

FIG. 5. Radial distribution function for nanocrystalline argon with different grain sizes.

function of nanocrystalline argon becomes closer to that of single crystal argon, indicating that the grain boundary structure has less influence on the overall structure.

Another function used to analyze the atomic structure is similar to x-ray diffraction, which is defined as[20]

$$\Phi = \frac{1}{N}\left|\sum_k e^{i2\pi\cdot 2r_{k,m}/\lambda}\right|, \tag{11}$$

where $r_{k,m}$ is the position of atom k in the m (x, y, or z) direction, N is the number of atoms under consideration, and λ is the wavelength of light. In this work, λ is chosen as the value of the lattice constant. The value of Φ represents the intensity of the light after diffraction. The value of Φ is not only determined by the crystallinity of the material, but also by the local crystallographic orientation. Figure 6 shows the

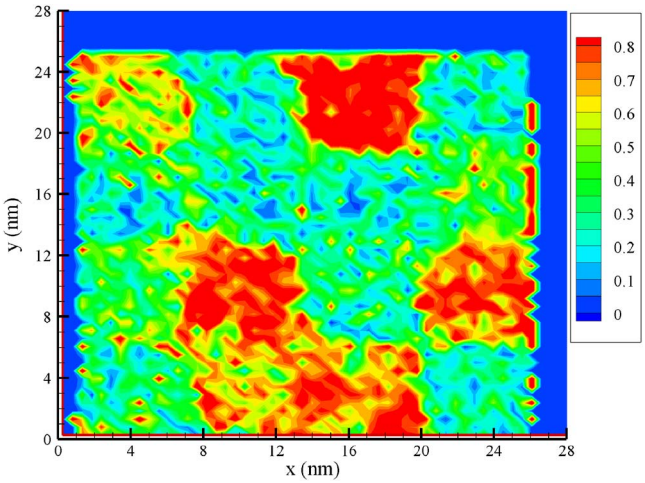

FIG. 6. (Color online) The Φ values for the nanocrystalline argon with 6.426 nm grains.

Φ values in the x direction for the nanocrystalline argon shown in Fig. 3. In this figure, four grains in each direction and grain boundaries could be observed clearly. Because of the different crystallographic orientations in the grains, the value of Φ is different for each of them.

B. Energy distribution

In addition to the radial distribution function, the energy distribution function is explored as well, which is defined as the fractional number of the atoms within a small energy range. Figure 7 shows the energy distribution function (EDF) of atoms within nanocrystalline argon with different grain sizes. For purpose of comparison, the atomic energy distribution function in single crystal film is shown in Fig. 7 as well. For single crystal argon, the peak for EDF appears at −1.87 (arbitrary unit). For nanocrystalline materials, it is evident that this peak is shifted to a higher level. For example, for the nanocrystalline argon with 2.14 nm grains, this peaks is at ~−1.8. This peak energy shift is attributed to the high energy of atoms in the grain boundary region. In this region, the atomic structure becomes loose to accommodate the crystallographic orientation change from one grain to the other one. As a result, the potential energy of the atoms will become large. With increasing grain size, the surface-to-volume ratio becomes smaller for the nanograins. Consequently, the effect of these interfacial atoms on the energy distribution becomes weaker, which is consistent with the results shown in Fig. 7.

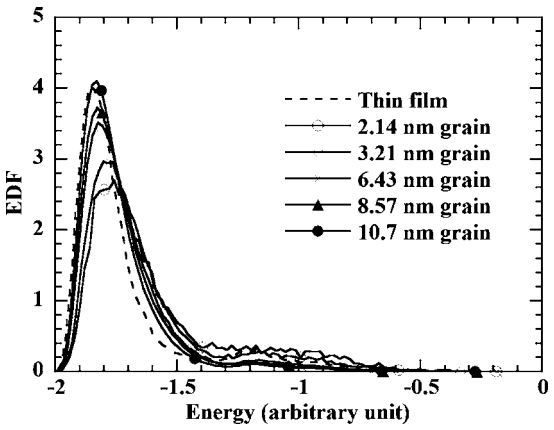

FIG. 7. Energy distribution function (EDF) of nanocrystalline materials.

Since nanocrystalline materials consist of nanoparticles compacted together, it would be of great interest to see the structural difference between single freestanding nanoparticles/nanograins and nanocrystalline materials. To this end, we study the energy distribution of atoms in a freestanding single argon nanoparticle at 30 K. The results as well as the comparison with a single crystal argon film are shown in Fig. 8. In Fig. 8(a), the curve shows the result for a nanoparticle with quite small diameter (2.14 nm). It is clear that the energy distribution is irregular due to the small number of atoms within the particle and the significant effect of free boundary condition at the particle surface. In addition, the energy distribution curve for the nanoparticle of 2.14 nm size is quite different from that of nanocrystalline materials of 2.14 nm grain size. This could be largely due to the free surface of nanoparticles. With increasing diameter, as shown in Figs. 8(a) and 8(b), the boundary effect becomes insignificant and the energy distribution function is in good agreement with that for the thin film. One clear observation is that for small nanoparticles, the fraction of atoms at higher energy levels becomes larger, which is similar to that observed in nanocrystalline materials.

C. Thermal conductivity

In this work, nanocrystalline argon with grain sizes from 2.142 to 10.71 nm is studied. Figure 9 shows the autocorrelation function of the heat flux versus time for a nanocrystalline argon sample with nanograins of 8.568 nm size. The variation trends in the three directions are close to each other, demonstrating the isotropic nature of thermal transport in the material. In the first short-time part (before 1.2 ps), all of the three curves have the exponential shape. In the long-time part (after 1.2 ps), the autocorrelation function tends to be zero with fluctuations. In the past, heat flux decay has been studied when calculating the thermal conductivity of materials using the Green-Kubo method in MD simulations.[21–23] In the work by Ladd *et al.*,[23] detailed discussions were provided about the heat flux decay and its oscillatory behavior. The fluctuation observed in Fig. 9 is induced by the rapid transport of energy back and forth over microscopic distances, and can be averaged out by transforming the $\langle q(t)q(0)\rangle \sim t$ curve to a phonon basis.[23] The fluctuation shown in Fig. 9 is less than that observed in the work by Ladd *et al.*,[23] probably due to the different system under study. The system studied by Ladd *et al.*[23] is characterized with an inverse-twelfth-power potential $\varepsilon(\sigma/r)^{12}$, which only gives rise to repulsive force between atoms. The system studied in this work has both repulsive and attractive forces between atoms. This will reduce the rapid back and forth energy transport between atoms and will lead to less fluctuation in the heat flux autocorrelation.

In order to calculate the thermal conductivity of the nanocrystalline material, long-time computation is needed in order to suppress the statistical uncertainty. Figure 10 shows

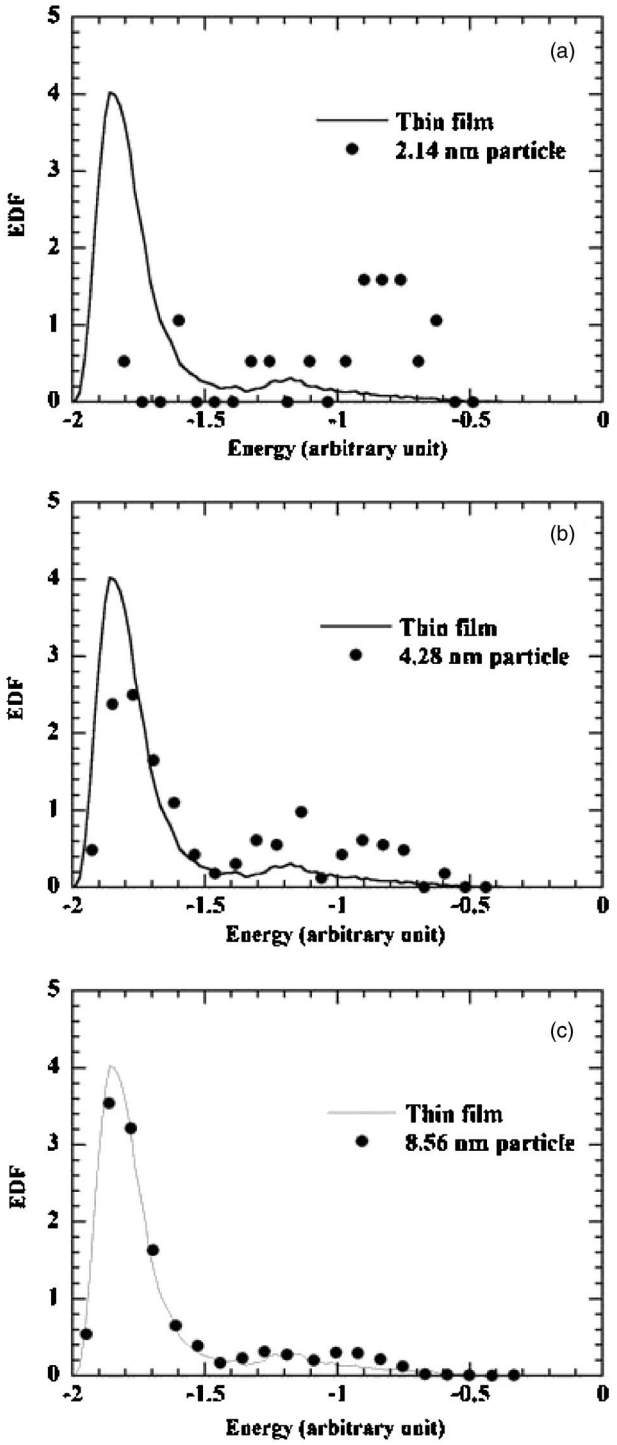

FIG. 8. Energy distribution function (EDF) of freestanding nanoparticles of different sizes.

the evolution of the thermal conductivity of the nanocrystalline argon with nanograins of 8.568 nm size. It is found that the thermal conductivities in the three directions are almost the same, which is due to the fact that the dimensions of the nanograin in the three directions are close to each other. It also indicates when the computational time approaches 2 ns, the thermal conductivities tend to be stable, meaning that 2 ns is long enough for the simulation of the thermal transport in nanocrystalline argon.

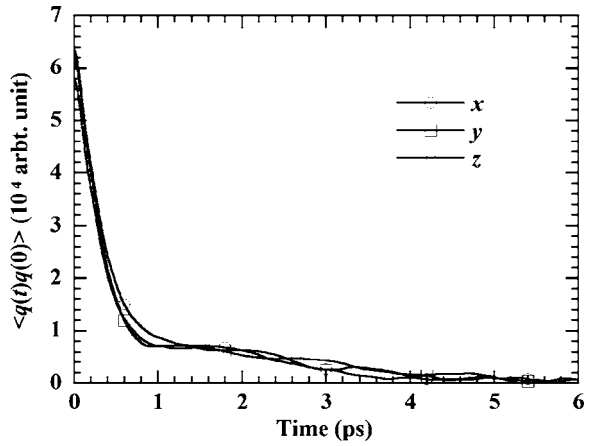

FIG. 9. The autocorrelation function of heat flux for nanocrystalline argon consisting of nanograins of 8.568 nm size.

As expected, the size of nanograins will have significant effect on the thermal transport in nanocrystalline materials. The variation of the thermal conductivity versus the nanograin size is shown in Fig. 11. Since the thermal conductivities in the three directions are close to each other, only the value in the *y* direction is presented in Fig. 11. It is seen that with increasing nanograin size, the thermal conductivity increases. Compared with our previous result for freestanding nanoparticles consisting of single crystals,[24] it is found that the thermal conductivity of nanocrystalline materials is a little larger than that of nanoparticles with the same characteristic size. The possible reason is that the nanograins in the nanocrystalline materials under study are not exactly spheres, but close to cubes. This could permit some low frequency phonons in the diagonal directions of the grains. Another reason is that for freestanding nanoparticles, the scattering at the boundary is total reflection, whereas for nanograins in nanocrystalline materials, some phonons can penetrate the boundary. As a result, there will be less reduction in thermal transport by boundary scattering in nanocrystalline materials. For the thermal conductivity reduction observed in Fig. 11, in addition to phonon scattering by the structure disorder at grain boundaries, there could be some other mechanisms contributing to the decrease in thermal

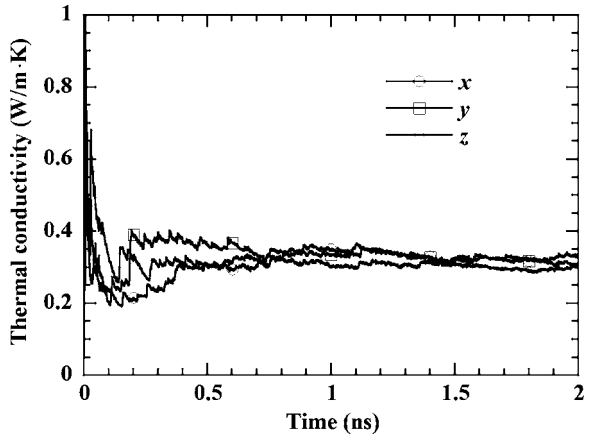

FIG. 10. Thermal conductivity of nanocrystalline argon with grain size 8.568 nm.

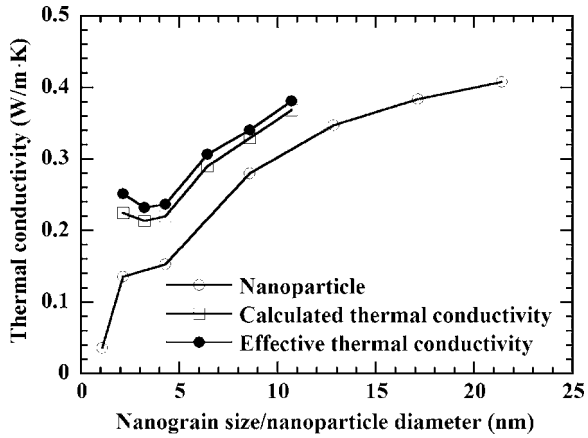

FIG. 11. Variation of the thermal conductivity vs the characteristic size of nanocrystalline materials and nanoparticles.

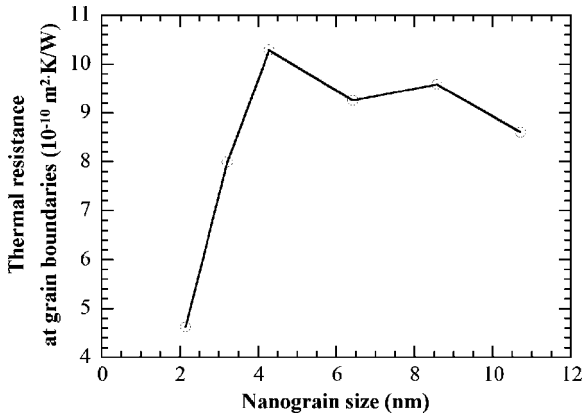

FIG. 12. Variation of the boundary thermal resistance vs the grain size.

conductivity. For example, due to the small size of nanograins, low frequency phonons are prohibited. This will reduce the thermal conductivity to a certain extent. In nanocrystalline materials, the crystallographic orientation is discontinuous across the grain boundary, leading to local acoustic mismatch. When phonons reach the grain boundary, both reflection and transmission take place. This means that the thermal energy cannot go from one grain to the other one freely. As a result, some boundary thermal resistance will arise and contribute to the overall thermal conductivity reduction observed in Fig. 11.

As discussed in Sec. III A, in comparison with the bulk counterpart, the nanocrystalline material has a density reduction due to the local disorder at grain boundaries. The density reduction becomes larger for nanocrystalline materials comprised of smaller grains. Part of the thermal conductivity reduction observed in Fig. 11 is attributed to the low density of the nanocrystalline material. In order to rule out the effect of the density on the thermal conductivity reduction, Maxwell's method[25] is applied to calculate the effective thermal conductivity of nanocrystalline argon assuming full density of the single crystal counterpart. The Maxwell equation considering the effect of cavities on the overall thermal conductivity is expressed as

$$\frac{k_{\mathrm{cal}}}{k_{\mathrm{eff}}} = 1 + \frac{3(\alpha - 1)\varphi}{(\alpha + 2) - (\alpha - 1)\varphi}, \tag{12}$$

where α is the ratio of thermal conductivity of cavities to the thermal conductivity of nanocrystalline argon (α=0 for this work), φ is the volume fraction of the cavity, k_{cal} is the calculated thermal conductivity, and k_{eff} is the effective thermal conductivity of nanocrystalline argon without cavities.

The result (effective thermal conductivity) is shown in Fig. 11. It is observed that after taking out the density effect, the effective thermal conductivity of nanocrystalline argon becomes slightly greater. On the other hand, the thermal conductivity of nanocrystalline argon is still much less than that of the bulk counterpart. This indicates that in comparison with the cavities in the nanocrystalline material, the grain boundary is a more important factor for the thermal conductivity reduction observed in this work. The presence of phonon scattering at grain boundaries will give rise to a boundary thermal resistance R. Assuming the nanograin itself has the same thermal conductivity as the bulk counterpart, the effective thermal conductivity of nanocrystalline materials is related to the boundary thermal resistance as[3]

$$k_{\mathrm{eff}} = \frac{k_0}{1 + (k_0 R/d)}, \tag{13}$$

where d is the nanograin size and k_0 is the thermal conductivity of bulk argon. In this work, k_0 takes the value of 0.55 W/m K based on our previous MD work on thermal transport in nanoscale argon at 30 K.[24] It needs to be pointed out that Eq. (13) is derived from Fourier's law.[3] When the nanograin size is extremely small, the uncertainty induced by the heat transfer deviation from the Fourier's law could be significant. The boundary thermal resistance reported here includes the effect of the non-Fourier thermal transport in nanograins. The variation of the boundary thermal resistance versus the grain size is calculated based on the effective thermal conductivity (shown in Fig. 11) and is plotted out in Fig. 12. The result shows that the thermal resistance at grain boundaries is not constant over the grain sizes studied in this work. It is in the order of 10^{-9} m^2 K/W. For smaller grain sizes, the calculated boundary resistance is smaller.

D. Specific heat

In addition to thermal conductivity, the specific heat of nanocrystalline argon is also studied in this work. Figure 13 shows the evolution of the specific heat for nanocrystalline argon consisting of 6.426 nm nanograins. Since the specific heat is calculated from the average of the fluctuation in the total energy, its value vibrates substantially when the computational time is short. With the time advancing, the specific heat features little variation around an equilibrium value. It is found that the specific heat of nanocrystalline argon is of the same order of magnitude as that of single crystal ($\sim$550 J/kg K).[24] Figure 14 shows the variation of the specific heat against the size of nanograins. It is observed that the specific heat of nanocrystalline argon does not change much with the size of nanograins. When the nanograin size becomes small ($\sim$3 nm), a slight decrease of the specific heat is observed.

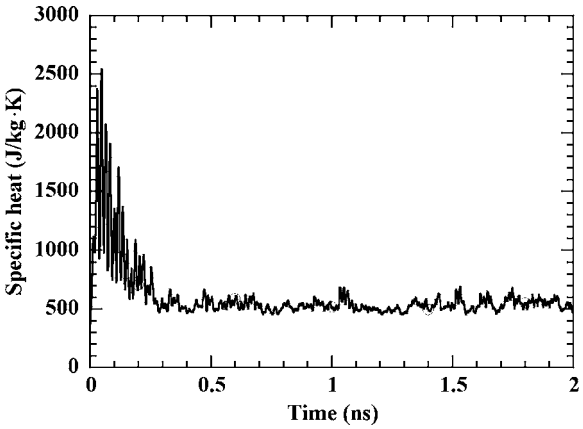

FIG. 13. Evolution of the specific heat of the nanocrystalline argon with nanograins of 6.426 nm size.

IV. CONCLUSION

In this work, the thermal transport in nanocrystalline argon was investigated using parallel MD simulation. It was found that the size of nanograins strongly affected the movement of phonons, thereby reducing the thermal conductivity of nanocrystalline materials. The thermal conductivity reduction observed in this work was mostly induced by the presence of grain boundaries and the small size of nanograins, while the small cavities with a small fraction in nanocrystalline materials had relatively small effect on thermal conductivity reduction. The thermal conductivity of nanocrystalline materials was a little larger than that of freestanding nanoparticles of single crystal with the same characteristic size. This could be attributed to some allowable low frequency phonons in the diagonal direction of nanograins and the transmission behavior of phonons at grain boundaries. The thermal resistance at grain boundaries was found to be in the order of 10^{-9} m^2 K/W. It is observed that when the grain size became smaller, the boundary thermal resistance became smaller as well. The specific heat of nanocrystalline materials was close to that of the single crystal material and showed little change with the grain size.

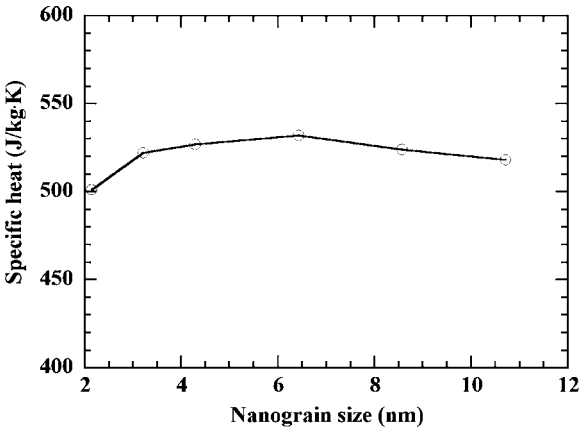

FIG. 14. Variation of the specific heat vs the nanograin size.

ACKNOWLEDGMENTS

Supports for this work from NSF (CTS: 0400458), Nebraska Research Initiative, and Layman Award of the University of Nebraska-Lincoln are gratefully acknowledged.

[1] C. W. Nan and R. Birringer, Phys. Rev. B **57**, 8264 (1998).
[2] G. Soyez *et al.*, Appl. Phys. Lett. **77**, 1155 (2000).
[3] H. Yang, G. R. Bai, L. J. Thompson, and J. A. Eastman, Acta Mater. **50**, 2309 (2002).
[4] J. Philip, P. Hess, J. E. Bulter, S. Chattopadhyay, K. H. Chen, and L. C. Chen, J. Appl. Phys. **93**, 2164 (2003).
[5] B. Peng, M. Cai, G. Li, X. J. Wu, and F. Zhou, Nanostruct. Mater. **4**, 475 (1994).
[6] H. V. Swygenhoven, D. Farkas, and A. Caro, Phys. Rev. B **62**, 831 (2000).
[7] K. Zhang, I. V. Alexandrov, R. Z. Valiev, and K. Lu, J. Appl. Phys. **80**, 5617 (1996).
[8] Y. Champion and M. J. Hÿtch, Eur. Phys. J.: Appl. Phys. **4**, 161 (1998).
[9] X. J. Wu, L. G. Du, H. F. Zhang, J. F. Liu, Y. S. Zhou, Z. Q. Li, L. Y. Xiong, and Y. L. Bai, Nanostruct. Mater. **12**, 221 (1999).
[10] M. Kobiyama, T. Inami, and S. Okuda, Scr. Mater. **44**, 1547 (2001).
[11] J. Schiøtz, F. D. D. Tolla, and K. W. Jacobsen, Nature (London) **391**, 561 (1998).
[12] C. J. Youngdahl, J. R. Weertman, R. C. Hugo, and H. H. Kung, Scr. Mater. **44**, 1475 (2001).
[13] Y. Champion, C. Langlois, S. Guérin-Mailly, P. Langlois, J. Bonnentien, and M. J. Hÿtch, Science **300**, 310 (2003).
[14] K. Pękala and M. Pękala, Nanostruct. Mater. **6**, 819 (1995).
[15] Y. K. Huang, A. A. Menovsky, and F. R. Boer, Nanostruct. Mater. **2**, 505 (1993).
[16] M. P. Allen and D. J. Tildesley, *Computer Simulation of Liquids* (Clarendon, Oxford, 1987).
[17] X. Wang and X. Xu, J. Heat Transfer **124**, 265 (2002).
[18] S. Volz, J. B. Saulnier, M. Lallemand, B. Perrin, P. Depondt, and M. Mareschal, Phys. Rev. B **54**, 340 (1996).
[19] S. R. Phillpot, D. Wolf, and H. Gleiter, J. Appl. Phys. **78**, 847 (1995).
[20] X. Wang and Y. Lu, J. Appl. Phys. **98**, 114304 (2005).
[21] A. J. H. McGaughey and M. Kaviany, Int. J. Heat Mass Transfer **47**, 1783 (2004).
[22] A. J. H. McGaughey and M. Kaviany, Int. J. Heat Mass Transfer **47**, 1799 (2004).
[23] A. J. C. Ladd, B. Moran, and W. G. Hoover, Phys. Rev. B **34**, 5058 (1986).
[24] Z. Zhong, X. Wang, and J. Xu, Numer. Heat Transfer, Part B **46**, 429 (2004).
[25] X. Wang, X. Xu, and S. U. S. Choi, J. Thermophys. Heat Transfer **13**, 474 (1999).